Applied Mathematical Modelling 69 (2019) 714–722

Contents lists available at ScienceDirect

Applied Mathematical Modelling

journal homepage: www.elsevier.com/locate/apm

Indirect diffusion based level set evolution for image segmentation

Yan Wang[a], Quan Yuan[a], Chuanjiang He[b,*]

[a] School of Mathematical Sciences, Chongqing Normal University, Chongqing 401331, China
[b] College of Mathematics and Statistics, Chongqing University, Chongqing 401331, China

ARTICLE INFO

Article history:
Received 19 June 2018
Revised 21 December 2018
Accepted 17 January 2019
Available online 30 January 2019

Keywords:
Image segmentation
Active contour
Level set
Diffusion
Transition region

ABSTRACT

In this paper, we put forward an idea of indirect diffusion and further develope an indirect diffusion-based level set model for image segmentation. This model is based on the dynamic process of diffusion that is posed indirectly on level set function by way of auxiliary function, coupled with a transition region-based force that exhibits the desired sign-changing property. It is formulated as a coupled system of two evolution equations, in which the first equation drives the motion of zero level set toward the object edges and makes it possible to set a termination criterion on the algorithm, while the second equation (indirect diffusion) smoothens the auxiliary function and keeps the auxiliary function as close to the level set function as possible. The derived model can effectively be solved purely by the simplest explicit finite difference. Experimental results show that the proposed model not only has the strong capability of noise immunity, but it also can much better conduce to extraction of deeply concave edges and preservation of sharp corners, compared with the direct diffusion-based counterpart.

1. Introduction

Image segmentation plays an important role in image analysis and computer vision. So far, a wide variety of segmentation techniques have been proposed in the literature, among which active contour models implemented via level set methods have been proved to be one of the most efficient methods. The main idea is that a contour is represented by the zero level of a higher dimensional function (called level set function), and the motion of contour is usually formulated as the evolution of level set function according to a partial differential equation (PDE).

Depending on different ways of deriving level set evolution (LSE) equation, level set based methods could be categorized into two classes: PDE-based [1–6] and variational models [7–13]. The PDE-based LSE is directly derived from the geometric consideration of evolution equations, while variational LSE is derived by minimization of an appropriately chosen energy functional over a function space.

So far, there have been a lot of works for PDE-based LSE, in which the evolution equations for level set function are usually derived by the curve evolution [1,3,5,6] or diffusion [2,4,14–16].

For the LSE by curve evolution, many models (e.g., [1,3,5,6]) are designed based on the motion by mean curvature, i.e., $\partial\phi/\partial t = div(\nabla\phi/|\nabla\phi|)|\nabla\phi|$, where ϕ is level set function. In fact, this equation represents a degenerate diffusion process,

* Corresponding author.
E-mail addresses: 20132095@cqnu.edu.cn (Y. Wang), cjhe@cqu.edu.cn (C. He).

https://doi.org/10.1016/j.apm.2019.01.020
0307-904X/

which diffuses ϕ in the direction orthogonal to its gradient $\nabla\phi$ and does not diffuse ϕ at all in the direction of $\nabla\phi$ [17], and hence makes ϕ smooth on both sides of the desired edge with a minimal smoothing of the edge itself.

For the LSE by diffusion, evolution equations for level set function are designed directly based on diffusion process. Motivated by the reaction-diffusion (RD) based phase transition theory [18], Zhang et al. [2] introduced the diffusion term $\varepsilon\Delta\phi$ into the conventional LSE equation and constructed the following RD equation:

$$\begin{cases} \frac{\partial\phi}{\partial t} = \varepsilon\Delta\phi - \frac{1}{\varepsilon}L(\phi) \\ \phi(x,y,0) = \phi_0(x,y) \end{cases}, \tag{1}$$

where $\varepsilon > 0$ is a small constant, $L(\phi) = -F|\nabla\phi|$ for PDE-based level set methods or $L(\phi) = -F\delta(\phi)$ for variational level set models. The re-initialization procedure is completely eliminated from the RD method owe to the regularization of diffusion term. The method can be generalized to a unified framework whose LSE equation can be either PDE-based ones or variational ones. Besides, the RD-LSE model is computed by means of simple finite difference and shows very good performance on boundary antileakage.

The models mentioned above could be classified into the direct diffusion framework, in which the diffusion is directly posed on level set functions. However, as the evolution proceeds forward in time, the level set function could be excessively smoothed, and so fails to extract some typical edges (sharp corner, deeply concave edge, etc.).

Recently, Wu and He [19] proposed a variational level set model in indirect regularization framework for image segmentation. Instead of using direct regularization on level set function, they introduced an auxiliary function to regularize indirectly the level set function. They showed that the indirect regularization has some advantages over direct regularization theoretically and experimentally. Experimental results illustrate that this model can better handle images with high noise, angle and weak edges.

In this paper, inspired by Wu and He [19], we put forward an idea of indirect diffusion and further present an indirect diffusion-based level set model for image segmentation in which the diffusion is posed indirectly on level set function by way of an auxiliary function. The indirect diffusion can aid in extraction of deeply concave edges and preservation of sharp corners. Different from Wu and He [19], the proposed model is formulated as a coupled system of two PDEs. The first equation drives the motion of level set function to extract the object edges and makes it possible to set a termination criterion on our algorithm. The second equation realizes the indirect diffusion of level set function. The proposed model has several merits, such as zero initialization, free of re-initialization, noise immunity, extraction of deeply concave edges, preservation of sharp corners, and easy implementation.

The remainder of this paper is organized as follows. Section 2 introduces and analyses the proposed model. Section 3 gives numerical scheme. Section 4 presents experimental results on a set of synthetic and real images. This paper is summarized in Section 5.

2. The proposed model

2.1. Indirect diffusion

For a function $\varphi(x, y, t)$ of two spatial variables (x, y) and time variable t, the simplest diffusion equation is

$$\frac{\partial\varphi}{\partial t} = \mu\Delta\varphi, \tag{2}$$

with the initial condition $\varphi(x,y,0) = \phi(x,y)$, where $\mu > 0$ is the diffusion coefficient, and Δ denotes the Laplace operator. It describes the dynamic process of the diffusion that is posed on the function ϕ, which smoothens the function ϕ isotropically.

In this study, we propose the indirect diffusion equation as follows:

$$\frac{\partial\varphi}{\partial t} = \mu\Delta\varphi + \gamma(\phi - \varphi), \tag{3}$$

with the initial condition $\varphi(x,y,0) = 0$, where γ is a positive parameter. In (3), the diffusion term $\mu\Delta\varphi$ smoothens isotropically the function φ, and the source term $\gamma(\phi - \varphi)$ ensures that φ keeps close to ϕ; this is because if $\phi > \varphi$ (or $\phi < \varphi$), then $\gamma(\phi - \varphi) > 0$ (or < 0), and so the function φ increases (or decreases) to approximate the function ϕ. Therefore, the Eq. (3) with the initial condition $\varphi(x,y,0) = 0$ describes the dynamic process of the diffusion which is posed indirectly on ϕ by means of φ.

2.2. Description of the model

Our indirect diffusion-based level set model is derived from the dynamic process of diffusion posed indirectly on level set function by auxiliary function, coupled with a transition region-based force. It is thus formulated as a system of two evolution equations with respect to the level set function and the auxiliary function.

Let $I:\Omega\to\mathcal{R}$ be a given image, ϕ be a level set function and φ be an auxiliary function. The proposed model is expressed as the coupled system of evolution equations as follows:

$$\begin{cases}\frac{\partial\phi}{\partial t}=\lambda(\varphi-\phi)+F(I(x,y))\\ \frac{\partial\varphi}{\partial t}=\mu\Delta\varphi+\gamma(\phi-\varphi)\end{cases}\tag{4}$$

with the initial and boundary conditions:

$$\phi|_{t=0}=0,\quad \varphi|_{t=0}=0\,,\quad \left.\frac{\partial\varphi}{\partial n}\right|_{\partial\Omega}=0,$$

where λ is a positive constant and $F(I)$ is a sign-changing force.

In the first equation of (4), the term $\lambda(\varphi-\phi)$ guarantees that the difference $|\phi-\varphi|$ can tend to λ^{-1} as $t\to\infty$ (see Theorem 1 below), which make it possible to set a termination criterion on our algorithm (see Remark 2 below). The sign-changing force $F(I)$ drives the level set function ϕ to move up or down adaptively on the image domain and finally identify objects from background. An ideal sign-changing force means that it has opposite sign inside and outside the objects of interest. For example, a reduced form of this ideal force can be described as follows:

$$F(I(x,y))=\begin{cases}\pm1 & (x,y)\in\omega\\ \mp1 & (x,y)\in\Omega\backslash\omega\end{cases},\tag{5}$$

where $\omega\subset\Omega$ denotes the objects of interest.

The following result can make it possible to set a termination criterion on our algorithm.

Theorem 1. *If $\lim_{t\to\infty}\varphi(x,y,t)$ exists, and $F(I(x,y))$ is given in (5), then the solution $\phi(x,y,t)$ of the problem*

$$\begin{cases}\frac{\partial\phi}{\partial t}=\lambda(\varphi-\phi)+F(I(x,y))\\ \phi(x,y,0)=0\end{cases}\tag{6}$$

satisfies

$$\lim_{t\to\infty}|\phi(x,y,t)-\varphi(x,y,t)|=\lambda^{-1}.\tag{7}$$

Proof. We first consider the case of $(x,y)\in\omega$. By (5) we have

$$\frac{\partial\phi}{\partial t}=\lambda(\varphi-\phi)\pm1.$$

It is easily seen that

$$\frac{\partial}{\partial t}(e^{\lambda t}\phi)=\lambda e^{\lambda t}\left(\varphi\pm\frac{1}{\lambda}\right).$$

Integrating the above equality on $[0,t]$, we obtain

$$\phi(x,y,t)=\lambda\int_0^t e^{\lambda(\tau-t)}\left(\varphi(x,y,\tau)\pm\frac{1}{\lambda}\right)d\tau.$$

By the Hospital's rule, we have

$$\begin{aligned}\lim_{t\to\infty}\lambda\int_0^t e^{\lambda(\tau-t)}\left(\varphi(x,y,\tau)\pm\frac{1}{\lambda}\right)d\tau &=\lim_{t\to\infty}\frac{\lambda\int_0^t e^{\lambda\tau}\left(\varphi(x,y,\tau)\pm\frac{1}{\lambda}\right)d\tau}{e^{\lambda t}}\\ &=\lim_{t\to\infty}\varphi(x,y,t)\pm\frac{1}{\lambda}.\end{aligned}$$

Thus, we get

$$\lim_{t\to\infty}\phi(x,y,t)=\lim_{t\to\infty}\varphi(x,y,t)\pm\frac{1}{\lambda},\quad(x,y)\in\omega.$$

Similarly, we can obtain

$$\lim_{t\to\infty}\phi(x,y,t)=\lim_{t\to\infty}\varphi(x,y,t)\mp\frac{1}{\lambda},\quad(x,y)\in\Omega\backslash\omega$$

The equality (7) is thus derived. The proof is complete. □

Remark 1. If the term $\lambda(\varphi-\phi)$ is omitted, then problem (6) is reduced to $\frac{\partial\phi}{\partial t}=\pm1$ with the initial condition $\phi(x,y,0)=0$. The solution of this problem is $\phi(x,y,t)=\pm t$, and so $\lim_{t\to\infty}\phi(x,y,t)=\pm\infty$. In this case, it is difficult to set an appropriate termination criterion for the algorithm.

Remark 2. For $\lambda > 0$, due to $\lim_{t\to\infty} |\phi(x,y,t) - \varphi(x,y,t)| = \lambda^{-1}$, we define the "normalized step difference energy" (NSDE), following [20], as follows:

$$NSDE(t) = \frac{\sum_{(x,y)\in\Omega} \left(|\phi(x,y,t) - \varphi(x,y,t)| - \lambda^{-1}\right)^2}{\sum_{(x,y)\in\Omega} |\phi(x,y,t) - \varphi(x,y,t)|^2}, \tag{8}$$

Thus we can by (8) set the termination criterion for our algorithm; see Remark 4 below.

2.3. Definition of the sign-changing force

The sign-changing force $F(I)$ plays a key role in our model because it is responsible for the desired segmentation. The sign-changing property by (5) could force the level set function ϕ to adaptively move up or down on the image domain as the evolution proceeds forward in time; for instance, if a pixel point, $(x, y) \in \omega$, has intensity such that $F(I(x, y)) = +1$, then the force $F(I(x, y))$ will drive $\phi(x, y, t)$ to move upward at the point (x, y). This is just desirable in that, if ϕ moves upward (downward) in $\Omega\backslash\omega$ and moves downward (upward) in ω, then the zero level line of ϕ (starting with zero function) could be generated and finally becomes the contours separating objects of interest from background.

The force term $F(I)$ with the desired sign properties (5) could possibly be defined in various ways. In this study, it is defined by transition regions, based on our previous works [4,6], as follows:

$$F(I(x,y)) = sign(T - I(x,y)), \tag{9}$$

where T is the intensity average of transition regions extracted from the image $I(x, y)$.

The existence of transition regions was first demonstrated in [21]. Transition regions are geometrically located between the objects and their background, and consist of pixels having intermediate grey levels between those of the objects and of their background. Such regions have certain width due to sampling and exhibit frequent changes in grey levels. They have always the following properties [22]: (1) There are transition regions near edges whether for step edges or non-step edges. Transition regions around non-step edges have several pixels' width, while transition regions near step edges have at least one pixel's width. Generally, in real world images, due to the error of sampling, there is several pixels' width even around step edges. (2) Transition regions cover around the objects. Because the edges are the boundaries between the objects and their background, the extracted transition regions should cover around the objects. In other words, transition regions are those that always contain a few object points and a few background points.

Due to the above properties of transition regions, we show that $F(I)$ in (9) has surely the desired property for an ideal binary image that has different intensity values a and b in ω and $\Omega\backslash\omega$, respectively. Without loss of generality, we assume the objects are brighter than the background, i.e., $a > b$. Since transition regions always contain a few object points and a few background points, the value of T is naturally between the objects' intensity and the background's intensity, i.e., $b < T < a$. It is easily been seen that, if $(x, y) \in \omega$, then $I(x, y) = a > T$, and hence $F(I(x, y)) = sign(T - I(x, y)) = -1$; if $(x, y) \in \Omega\backslash\omega$, then $I(x, y) = b < T$, and so $F(I(x, y)) = +1$.

So far, a number of methods have been proposed to extract transition regions. In this study, we adopt the local entropy-based transition region extraction method (LE-TREM) proposed by Yan et al. [22]. This algorithm is listed in the following:

(1) Given certain neighbour window size and compute the local entropy for every pixel in image, then obtain the local entropy image $E(x, y)$.
(2) Compute the entropy image's maximal value $E_{\max}$, and determine the local entropy threshold by $E_T = \alpha E_{\max}$, where α is a coefficient between 0 and 1.
(3) Extract transition region.

The observation by experiments is that transition regions extracted by LE-TREM always contain several points of both object and background [6]. Obviously, only if the extracted region contains some pixels of both objects and background, then the corresponding intensity average of transition regions is between the objects' intensity and the background's intensity. Therefore, $T - I(x, y)$ will change the plus or minus sign when point (x, y) travels between the inside and outside of objects, and hence the condition (5) is satisfied, where T is the intensity average of transition regions extracted by LE-TREM.

3. Numerical implementation

We use the simplest explicit discrete approximation of (4) in order to show the independence of the proposed model on numerical schemes.

Let h be the space step and Δt be the time step, and $(x_i, y_j) = (ih, jh)$ be the grid points. Let $\phi^n_{i,j} = \phi(x_i, y_j, n\Delta t)$ and $\varphi^n_{i,j} = \varphi(x_i, y_j, n\Delta t)$ be the approximations of $\phi(x, y, t)$ and $\varphi(x, y, t)$, respectively, with $n \geq 0$, $\phi^0 = \phi_0$, $\varphi^0 = \varphi_0$. The spatial partial derivatives $\partial^2\varphi/\partial^2 x$ and $\partial^2\varphi/\partial^2 y$ are approximated by the central differences, and the temporal partial derivative $\partial\phi/\partial t$ and $\partial\varphi/\partial t$ are discretized by the forward differences. The discretizations of two differential equations in (4) can be written as

$$\phi^{n+1}_{i,j} = \phi^n_{i,j} + \Delta t \cdot \left(\lambda(\varphi^n_{i,j} - \phi^n_{i,j}) + sign(T - I_{i,j})\right) \tag{10}$$

and

$$\varphi_{i,j}^{n+1} = \varphi_{i,j}^{n} + \Delta t \cdot \left(\mu \left(\frac{\varphi_{i+1,j}^{n} + \varphi_{i-1,j}^{n} - 2\varphi_{i,j}^{n}}{h^2} + \frac{\varphi_{i,j+1}^{n} + \varphi_{i,j-1}^{n} - 2\varphi_{i,j}^{n}}{h^2} \right) + \gamma (\phi_{i,j}^{n} - \varphi_{i,j}^{n}) \right). \tag{11}$$

In summary, the algorithm for solving the model (4) is described in Algorithm 1 below.

Algorithm 1 The algorithm for solving the proposed model (4).

1. Initialize $\phi^n = \phi^0 = 0$, $\varphi^n = \varphi^0 = 0$, $n = 0$.
2. Compute the intensity average T of the transition region extracted by LE-TREM and then $F(I(x, y)) = sign(T - I)$.
3. Compute $\phi_{i,j}^{n+1}$ by (10) and $\varphi_{i,j}^{n+1}$ by (11).
4. Return to step 3 until the termination criterion is satisfied.

Remark 3. For our model (4), the initial functions of both ϕ and φ are chosen as zero functions, which implies that the model is actually free of initialization. Such zero initialization is efficient computationally and extremely convenient in practice. We do not need to consider the problems of where and how to define the initial contours. Although there exists no zero level line for such zero initialization, the zero level line of ϕ can be automatically generated due to the sign-changing property of $F(I(x, y))$.

Remark 4. As done in many level set models, we can also predefine a larger iteration number for our model to finally detect the desired objects. However, this is clearly time-consuming and cannot acquire the optimal speed. Fortunately, by Remark 2 we can set the following termination criterion for our algorithm.

The principal steps of the termination criterion are as follows:

(1) Predefine a threshold $\delta > 0$ and an iteration number $N > 0$.
(2) Compute $NSDE(n)$ by (8) and check whether $NSDE(n) \le \delta$, or $n \ge N$. If not, set $n = n + 1$ and repeat.

In our experiments, we use $\delta = 0.5$ and $N = 50$.

4. Experimental results

In this section, we first present a few numerical results to justify that the indirect diffusion by (3) is superior to the direct diffusion by (2) in terms of the extraction of both sharp corners and concave edges and has still the strong capability of noise immunity. Second, we evaluate the performance of our model on the binarization of document images, in comparison to three relevant models in [4,6,19], qualitatively and quantitatively. Finally, we show that the proposed model can be applied to segmentation of some other real-world images.

The parameters for our model are set as follows: $\mu = 5$, $\lambda = 1$, $\gamma = 0.01$, $\Delta t = 0.04$, $h = 1$. The parameter α should be chosen from the interval [0.4,0.99]; $\alpha = 0.99$ for Figs. 1–3, and α is adjusted according to different images for Figs. 4–6.

Firstly, we show that indirect diffusion by (3) has the advantages over direct diffusion by (2) (see Figs. 1 and 2) and the strong capability of noise immunity (see Fig. 3).

In the direct diffusion framework, the proposed model (4) is rewritten as

$$\frac{\partial \phi}{\partial t} = \mu \Delta \phi + sign(T - I). \tag{12}$$

It is also approximated by the simplest explicit discretization as follows:

$$\phi_{i,j}^{n+1} = \phi_{i,j}^{n} + \Delta t \cdot \left(\mu \left(\frac{\phi_{i+1,j}^{n} + \phi_{i-1,j}^{n} - 2\phi_{i,j}^{n}}{h^2} + \frac{\phi_{i,j+1}^{n} + \phi_{i,j-1}^{n} - 2\phi_{i,j}^{n}}{h^2} \right) + sign\left(T - I_{i,j}\right) \right). \tag{13}$$

For the space step $h = 1$, the time step Δt for this finite difference scheme must satisfy the Courant-Friedrichs-Lewy (CFL) condition for numerical stability: $\mu \Delta t < 0.25$. In our experiments, we still choose $\mu = 5$ and $\Delta t = 0.04$.

Fig. 1 demonstrates that the indirect diffusion model (4) can much better extract sharp corners than the direct diffusion model (12), in which an ideal binary image is chosen as the test image. The segmentation result of the model (12) is shown in the top row of Fig. 1. We can see that the corners are smoothed as the evolution proceeds, and the contour will finally disappear. By contrast, the model (4) extracts sharp corners effectively, as shown in the bottom row of Fig. 1. Moreover, the 3D-plot shown in Fig. 1(f) displays that the difference between the final level set and auxiliary functions, $\phi - \varphi$, really approaches to $\pm\lambda^{-1} = \pm 1$, which is in accordance with the theoretical result by Theorem 1.

Fig. 2 shows that the indirect diffusion model (4) can much better handle images with boundary concavities than the direct diffusion model (12). Two sample images are plotted in the first column of Fig. 2, which are a synthetic image with deep concavities and a dragon-like image with concavity and complex edges, respectively. The first and third rows of Fig. 2 present the segmentation results of the model (12) after 10, 100 and respectively 500 iterations. We can see that the concavities of zero level line will gradually disappear and the corners will be smoothed as the evolution proceeds. By contrast, as shown

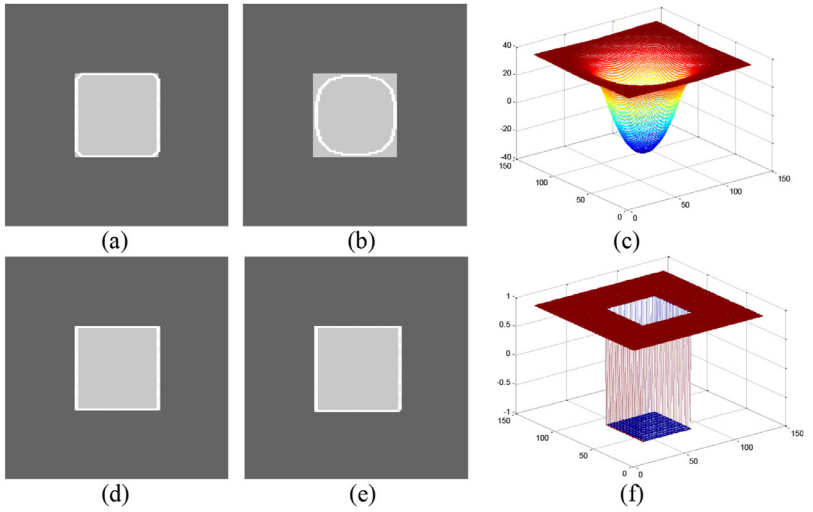

Fig. 1. Segmentation results of both direct diffusion-based model (Top row) and indirect diffusion-based model (Bottom row) for an ideal binary image. Columns 1–2: Segmentation results after 100 and respectively 1000 iterations; see the white contours superimposed on the original images. (c) in Column 3: level set function ϕ after 1000 iterations. (f) in Column 3: difference between level set function and auxiliary function, $\phi - \varphi$, after 1000 iterations.

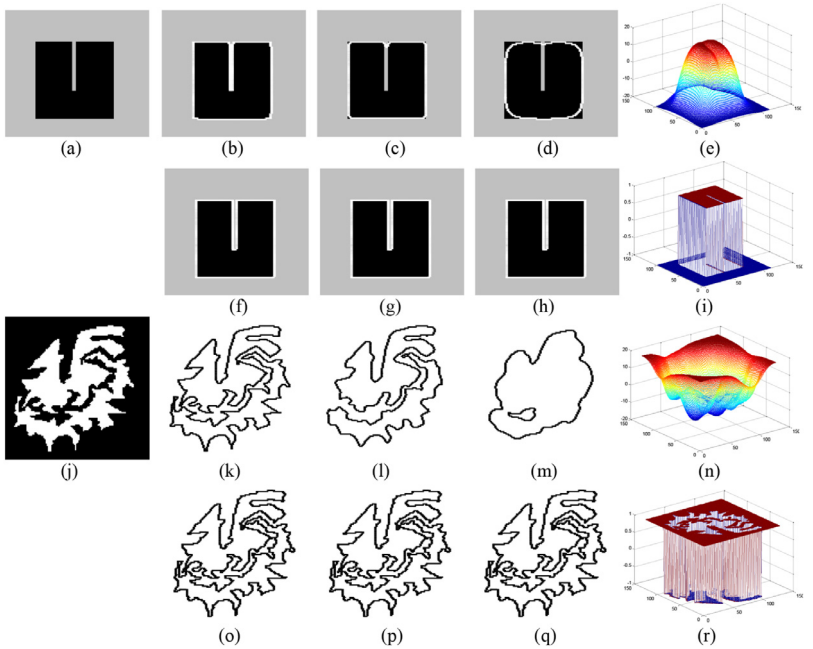

Fig. 2. Segmentation results of both direct diffusion-based model (rows 1 and 3) and indirect diffusion-based model (rows 2 and 4) for two images with deep boundary concavities. Column 1: original images. Columns 2–4: segmentation results after 10, 100 and respectively 500 iterations; see the white contours superimposed on the original image for first two rows and the black contours for last two rows. (e) and (n) in Column 5: level set function ϕ after 500 iterations. (i) and (r) in Column 5: difference between level set function and auxiliary function, $\phi - \varphi$, after 500 iterations.

in the second and fourth rows in Fig. 2, the model (4) exactly extracts both sharp corners and deeply concave edges in both images.

In Fig. 3, we show that the indirect diffusion model (4) also has the strong capability of noise immunity. The first row of Fig. 3 presents three noisy images with different noise levels. The segmentation results and the 3-D plot of $\phi - \varphi$ are shown in the second and third rows, respectively. We can see that the model (4) extracts successfully edge of the objects from these noisy images, and $\phi - \varphi$ converges to ± 1, as $t \to \infty$.

Secondly, we evaluate the performance of our model by applying it to the binarization of document images, in comparison to three related models in [4,6,19], subjectively and objectively.

The test images are chosen from the DIBCO (Competition on Document Image Binarization) testing datasets (2009 to 2014 and 2016). These datasets supply original images and their associated ground truths, which are convenient for

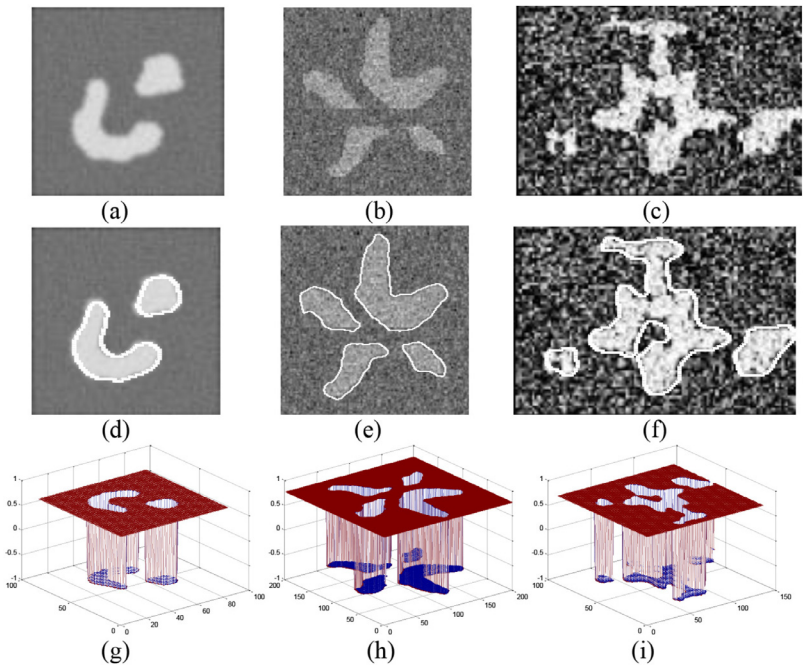

Fig. 3. Segmentation results of our model for noisy images. Row 1: original images. Row 2: segmentation results. Row 3: difference between the final level set function and auxiliary function, $\phi - \varphi$.

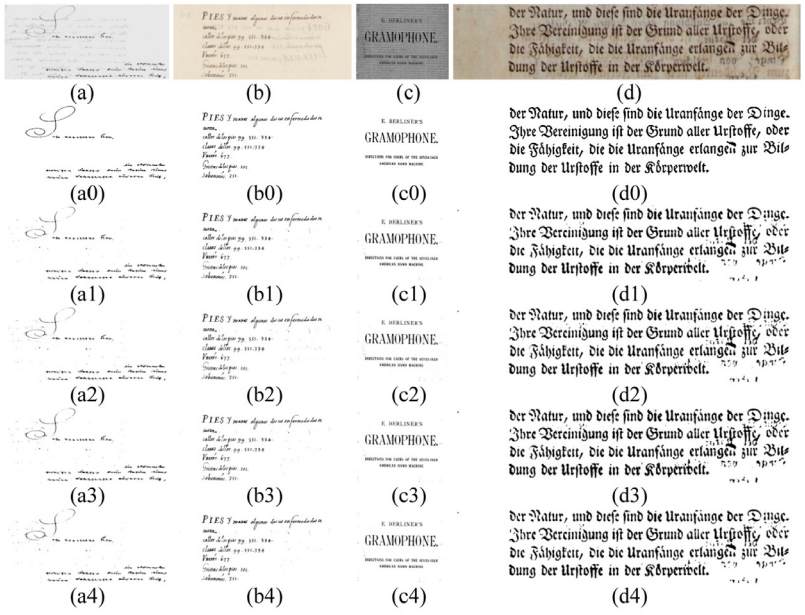

Fig. 4. Original images and binarization results by four models for four document images. Row 1: original images. Row 2: ground truths. Rows 3–6: results of the models in [4,6,19] and respectively our model.

quantitative evaluation. We adopt four measures to evaluate the performances of four models quantitatively. The four evaluation measures are F-Measure (FM), pseudo-FMeasure (Fps), Distance Reciprocal Distortion (DRD) and Peak Signal to Noise Ratio (PSNR), which are suitable for evaluation purposes in the context of document analysis and recognition [23].

In this experiment, we successively apply one of four models on the same document image and obtain the final level set function $\{\phi_{i,j}^N\}$. The binarized versions of this document image are then obtained by the following projection:

$$B(i,j) = \begin{cases} +1, & \text{if } \phi_{i,j}^N > 0 \\ -1, & \text{if } \phi_{i,j}^N \le 0 \end{cases} \tag{14}$$

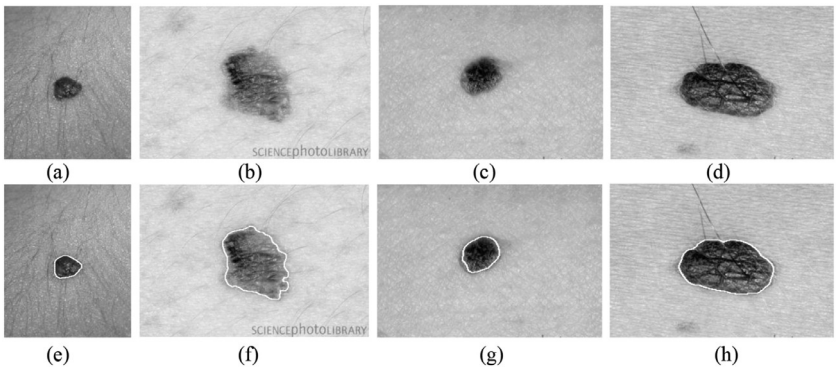

Fig. 5. Segmentation results of our model for four skin lesion images. Row 1: original images. Row 2: segmentation results;see the white contours superimposed on the original images.

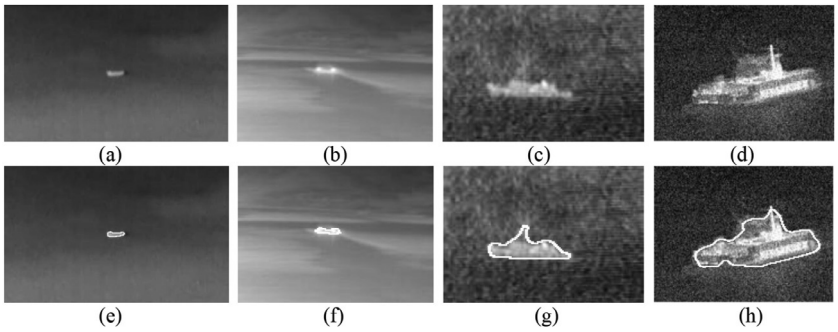

Fig. 6. Segmentation results of the proposed model on real infrared ship images. Row 1: original images. Row 2: segmentation results; see the white contours superimposed on the original images.

where the values $+1$ and -1 mean background (in white) and texts (in black), respectively. We display the final binarization by $\{B(i, j)\}$ instead of the zero level line of $\{\phi_{i,j}^N\}$.

In Fig. 4, we display the binarization results of four models for two handwritten document images and two machine printed document images. For our model, we set the parameter $\alpha = 0.79, 0.78, 0.94$ and 0.83 for these document images. For other three comparison models, we refer to their corresponding papers and adjust the parameters as well as iteration numbers so that they can obtain the best results. In detail, for the model in [4], we use $\lambda = 0.78, 0.77, 0.94$ and 0.82 with iterations numbers 4, 1, 2 and 2, respectively. For the model in [6], we use $\alpha =$ 0.82, 0.99, 0.99 and 0.85 with iteration numbers 2, 3, 3 and 3, respectively. For the model in [19], we use $\lambda_1 = 1, \lambda_2 = 0.5$; $\lambda_1 = 1, \lambda_2 = 0.9$; $\lambda_1 = 0.5, \lambda_2 = 1$; $\lambda_1 = 1, \lambda_2 = 1$ with iteration numbers 21, 20, 20 and 22, respectively.

The first and second rows of Fig. 4 show the original images and the corresponding ground truths, respectively. The binarization results by the models in [4,6,19] and our model are shown in Rows 3–6 of Fig. 4, respectively. The corresponding evaluation measure values are listed in Table 1. From Fig. 4, we can observe that the four models have visually almost same binarization results for these document images. However, it can be seen from Table 1 that our model has the best values of the used measures as a whole.

Finally, we demonstrate that the proposed model can be applied to segmentation of some other real-world images.

Fig. 5 shows segmentation results of our model for four real skin lesion images which are taken from Science Photo Library (http://www.sciencephoto.com). Detecting skin lesion edges is a basic step in computer-aided lesion analysis. However, the detection of edges is a challenging computer vision problem due to the variability in shape and appearance of skin lesions. Other factors such as the presence of noise and hair also make the segmentation process more difficult [24]. For these images, we choose $\alpha = 0.98, 0.8, 0.99,$ and 0.87, respectively. The first row of Fig. 5 shows the original skin lesion images, and the corresponding segmentation results are displayed in the second row. We can observe that the proposed model obtains satisfactory segmentation results for all these images.

In Fig. 6, we show segmentation results of our model for four real infrared ship images. As shown in the top row, these images suffer from low intensity contrast with weak boundaries or noise. From the bottom row, we observe that the proposed model ($\alpha = 0.95, 0.96, 0.92, 0.91$) successfully extracts the desired objects from the complex backgrounds for all these images.

Table 1
Evaluation measure values of four models for Fig. 4.

Image ID		(a)	(b)	(c)	(d)
FM(%)	[4]	87.3819	93.8801	91.4845	86.3071
	[6]	87.676	93.8628	91.3199	86.6513
	[19]	87.6504	94.2319	91.3684	86.7373
	Ours	**87.8447**	**94.2512**	**91.5593**	**86.8133**
F_{ps}(%)	[4]	**90.1826**	96.9662	**93.4342**	89.0446
	[6]	89.4033	95.4599	91.678	88.9335
	[19]	89.5456	**97.08**	92.4248	88.0787
	Ours	89.5443	96.1754	93.1524	**89.8055**
DRD	[4]	4.4897	1.6652	3.5759	4.1777
	[6]	4.1519	1.5241	3.5696	3.9355
	[19]	4.4266	1.4766	3.4949	4.2357
	Ours	**4.1475**	**1.4304**	**3.4145**	**3.8425**
PSNR	[4]	22.845	24.3547	20.7946	13.9525
	[6]	22.9791	24.2627	20.6343	14.0661
	[19]	22.8868	**24.6134**	20.7232	13.9562
	Ours	**23.0147**	24.5766	**20.8465**	**14.176**

5. Conclusion

In this paper, following the idea of indirect diffusion, we propose an indirect diffusion-based level set evolution model using coupled PDEs for image segmentation. The indirect diffusion together with sign-changing force can much better conduce to deeply concave edges extraction and sharp corners preservation, compared to the direct diffusion-based counterpart. The derived model can effectively be solved purely by the simplest explicit finite difference. Experimental results display the good performance of our model.

Acknowledgments

This work was partially supported by the Chinese National Science Foundation (Grant no. 61561019), National Natural Science Foundation of China (Grant no. 61561019), the Natural Science Foundation Project of CQ CSTC (cstc2015jcyjA00019) and the Science and Technology Research Program of Chongqing Municipal Education Commission (KJQN201800537, KJZD-M201800501).

References

[1] V. Caselles, F. Catte, T. Coll, F. Dibos, A geometric model for active contours in image processing, Numer. Math. 66 (1) (1993) 1–31.
[2] K. Zhang, L. Zhang, H. Song, D. Zhang, Reinitialization-free level set evolution via reaction diffusion, IEEE Trans. Image Process. 22 (1) (2013) 258–271.
[3] Y. Wang, C. He, Adaptive level set evolution starting with a constant function, Appl. Math. Model. 36 (2012) 3217–3228.
[4] W. Wen, C. He, Y. Zhang, Z. Fang, A novel method for image segmentation using reaction-diffusion model, Multidim. Syst. Sign. Process. 28 (2) (2017) 657–677.
[5] K. Zhang, L. Lei, H. Song, W. Zhou, Active contours with selective local or global segmentation: a new formulation and level set method, Image Vis. Comput. 28 (4) (2010) 668–676.
[6] W. Wen, C. He, M. Li, Transition region-based active contour model for image segmentation, J. Electron. Image 22 (1) (2013). 013021 (Jan-Mar).
[7] C. Li, C. Xu, C. Gui, M.D. Fox, Distance regularized level set evolution and its application to image segmentation, IEEE Trans. Image Process. 19 (12) (2010) 3243–3254.
[8] T. Chan, L. Vese, Active contours without edges, IEEE Trans. Image Process. 10 (2) (2001) 266–277.
[9] Y. Wu, M. Li, Q. Zhang, Y. Liu, A Retinex modulated piecewise constant variational model for image segmentation and bias correction, Appl. Math. Model. 54 (2018) 697–709.
[10] Y. Zhao, S. Guo, M. Luo, X. Shi, M. Bilello, S. Zhang, C. Li, A level set method for multiple sclerosis lesion segmentation, Mag. Reson. Imaging 49 (2018) 94–100.
[11] K. Ding, L. Xiao, G. Weng, Active contours driven by local pre-fitting energy for fast image segmentation, Pattern Recognit. Lett. 104 (2018) 29–36.
[12] C. Huang, L. Zeng, Level set evolution model for image segmentation based on variable exponent p-laplace equation, Appl. Math. Model. 40 (17–18) (2016) 7739–7750.
[13] B. Zhou, C. Mu, Level set evolution for boundary extraction based on a p-laplace equation, Appl. Math. Model. 34 (12) (2010) 3910–3916.
[14] B. Chen, Y. Li, J. Cai, Noisy image segmentation based on nonlinear diffusion equation model, Appl. Math. Model. 36 (3) (2012) 1197–1208.
[15] B.A. Jacobs, E. Momoniat, A novel approach to text binarization via a diffusion-based model, Appl. Math. Comput. 225 (2013) 446–460.
[16] B.A. Jacobs, E. Momoniat, A locally adaptive, diffusion based text binarization technique, Appl. Math. Comput. 269 (2015) 464–472.
[17] L. Alvarez, P.L. Lions, J.M. Morel, Image selective smoothing and edge detection by nonlinear diffusion. II, SIAM J. Numer. Anal. 29 (3) (1992) 845–866.
[18] G. Barles, L. Bronsard, P. Souganidis, Front propagation for reaction-diffusion equations of bistable type, Ann. Inst. Henri Poincare 9 (5) (1992) 479–496.
[19] Y. Wu, C. He, Indirectly regularized variational level set model for image segmentation, Neurocomputing 171 (2016) 194–208.
[20] S.H. Lee, J.K. Seo, Level set-based bimodal segmentation with stationary global minimum, IEEE Trans. Image Process. 15 (2006) 2843–2852.
[21] J.J. Gerbrands, Segmentation of noise images, Delft University, The Netherlands, 1988 Ph.d. dissertation.
[22] C. Yan, N. Sang, T. Zhang, Local entropy-based transition region extraction and thresholding, Pattern Recognit. Lett. 24 (16) (2003) 2935–2941.
[23] I. Pratikakis, K. Zagoris, G. Barlas, B. Gatos, ICFHR2016 handwritten document image binarization contest (h-DIBCO 2016), Proceedings of the 15th International Conference on Frontiers in Handwriting Recognition (2016) 619–623.
[24] C.A.Z. Barcelos, V.B. Pires, An automatic based nonlinear diffusion equations scheme for skin lesion segmentation, Appl. Math. Comput. 215 (2009) 251–261.